Journal of the European Ceramic Society

Synthesis of highly Li-ion conductive garnet-type solid ceramic electrolytes by solution-process-derived sintering additives

--Manuscript Draft--

Manuscript Number:	JECESOC-D-21-01141R2
Article Type:	Short Communication
Keywords:	garnet-type solid electrolyte, solution process, sintering additives, processing, sintering
Corresponding Author:	Nataly Carolina Rosero Navarro, Ph.D. Hokkaido University Sapporo, JAPAN
First Author:	Nataly Carolina Rosero Navarro, Ph.D.
Order of Authors:	Nataly Carolina Rosero Navarro, Ph.D.
	Haruna Watanabe
	Akira Miura
	Kiyoharu Tadanaga
Abstract:	The sintering and processing of garnet-type solid ceramic electrolytes (e.g., Li7La3Zr2O12 (LLZ)) are challenging because the material composition and microstructure at high temperatures must be carefully controlled to obtain the stabilization of highly conductive cubic phase and dense ceramic. Liquid-phase sintering using sintering aids is typically used for densifying ceramic materials, as it is a faster and/or lower-temperature process. In this study, we used solution-process-derived sintering additives to sinter garnet-type solid electrolytes highly effective in terms of relative density and properties at 1000 °C (10h). The liquid phase formation during the sintering was rationalized to establish the optimal sintering conditions. The use of 1.2-vol% 75Li2O•25B2O3 and 1.5-vol% Al2O3 as sintering additives was highly effective in densifying a Ta-doped LLZ, achieving a high ionic conductivity of 0.8 mScm −1 (25 °C) with low activation energy (9 kJ mol −1) and almost negligible contribution of the grain boundary resistance (10%).

Synthesis of highly Li-ion conductive garnet-type solid ceramic electrolytes by solution-process-derived sintering additives

Nataly Carolina Rosero-Navarro[a*], Haruna Watanabe[b], Akira Miura[a], and Kiyoharu Tadanaga[a]

[a]Division of Applied Chemistry, Faculty of Engineering, Hokkaido University, Kita 13 Nishi 8, Kita-ku, Sapporo 060–8628, Japan

[b]Graduate School of Chemical Sciences and Engineering, Hokkaido University, Kita 13 Nishi 8, Kita-ku, Sapporo 060–8628, Japan

*E-mail address: rosero@eng.hokudai.ac.jp, tel. +81-011-706-6574

Abbreviations

$Li_7La_3Zr_2O_{12}$ (LLZ); Ta-doped LLZ (LLZT); scanning electron microscopy (SEM); X-ray diffraction (XRD); $75Li_2O{\cdot}25B_2O_3$ (LBO); energy-dispersive spectroscopy (EDS).

Abstract

The sintering and processing of garnet-type solid ceramic electrolytes (e.g., $Li_7La_3Zr_2O_{12}$ (LLZ)) are challenging because the material composition and microstructure at high temperatures must be carefully controlled to obtain the stabilization of highly conductive cubic phase and dense ceramic. Liquid-phase sintering using sintering aids is typically used for densifying ceramic materials, as it is a faster and/or lower-temperature process. In this study, we used solution-process-derived sintering additives to sinter garnet-type solid electrolytes highly effective in terms of relative density and properties at 1000 °C (10 h). The liquid phase formation during the sintering was rationalized to establish the optimal sintering conditions. The use of 1.2-vol% $75Li_2O{\cdot}25B_2O_3$ and 1.5-vol% Al_2O_3 as sintering additives was highly effective in densifying a Ta-doped LLZ, achieving a high ionic conductivity of 0.8 mS cm^{-1} (25 °C) with low activation energy (9 kJ mol^{-1}) and almost negligible contribution of the grain boundary resistance (10%).

Keywords: garnet-type solid electrolyte, solution process, sintering additives, processing, sintering

Lithium-ion conductive solid ceramic electrolytes with a garnet structure (e.g., $Li_7La_3Zr_2O_{12}$ (LLZ)) are usually prepared by a solid-state reaction including several grinding and calcination steps with a final sintering at a temperature of approximately 1200 °C, in which a dense ceramic with a highly conductive cubic phase is obtained. At such temperatures, the control of the material composition and microstructure (lower contribution of the grain boundary resistance) is rather challenging considering the easy volatilization of lithium [1, 2].

Liquid-phase sintering is typically used for densifying ceramic materials at faster and/or low temperatures, which proceeds by mixing a low-melting-point sintering additive with ceramic particles sintered at a temperature equal to or higher than the melting point of the sintering additive. In the liquid-phase sintering, the liquid phase promotes shrinkage at the initial stage because of the rearrangement of the particles and dissolution and reprecipitation processes. Simultaneously, the surface energy tends to reduce the gas–liquid interface expelling the bubbles from the system. When the sintering temperature is reached, full densification of the ceramic is achieved. Al_2O_3 is a widely used sintering additive for garnet-type solid ceramic electrolytes, which changes both crystal grain composition and grain boundary. As the eutectic temperature of the Li_2O–Al_2O_3 binary system is approximately 1055 °C [3-5], the formation of this liquid phase promotes the sintering. Different sintering additives have been proposed [4-15]. Among them, Li_3BO_3 (with a content of approximately 6–10 wt%) is one of the most efficient additives to reduce the sintering temperature, as it is unreactive during sintering and enables to obtain relatively dense solid electrolytes at a temperature of 800 °C. Amorphous lithium borate is present at the triple-point grain boundaries. Li_3BO_3 is

presumably present at the interface as a layer at the grain boundaries between the LLZ particles. Large regions of lithium borate through the composite electrolyte have been observed [4, 16]. Therefore, the total lithium-ion conductivity of the composite solid electrolyte containing the sintering additive was strongly affected by the content of the sintering additive. As the lithium-ion conductivity of Li_3BO_3 is approximately 10^{-6} S cm^{-1} [17], the addition of a large amount of this sintering additive increases the resistance of the composite solid electrolyte, leading to a large decrease in the conductivity, while an insufficient amount leads to a poor densification and insufficient lithium pathway for the ionic conductivity [4, 8-10, 12, 13, 15].

In this study, we propose an alternative route to sinter garnet-type solid ceramic electrolytes using solution-process-derived sintering additives to overcome the limitations of current sintering additives. The use of solution-process-derived sintering additives enables a significant reduction in the sintering additive content, and thus a composite electrolyte in which the lithium-ion transport properties are attributed mainly to the highly conductive phase of the garnet solid electrolyte. We studied the effects of Li_2O–B_2O_3 and Al_2O_3 solution-derived sintering additives on the sinterability of a Ta-doped LLZ (LLZT). The effect of solution-derived sintering additives was compared to their powder-state counterparts. In addition, to strengthen the liquid-phase sintering, lanthanum oxide was used to modify the liquid phase generated at low temperatures because the eutectic temperature for binary systems such as $LiBO_2$–La_2O_3 can be as low as 710 °C [18]. Thus, 1.2-vol% (0.5 wt%) $75Li_2O{\cdot}25B_2O_3$ and 1.5-vol% Al_2O_3 as sintering additives are highly effective in densifying

an LLZT ceramic solid electrolyte achieving the highest ionic conductivity of 0.8 mS cm^{-1} at 25 °C reported for this type of composite electrolytes.

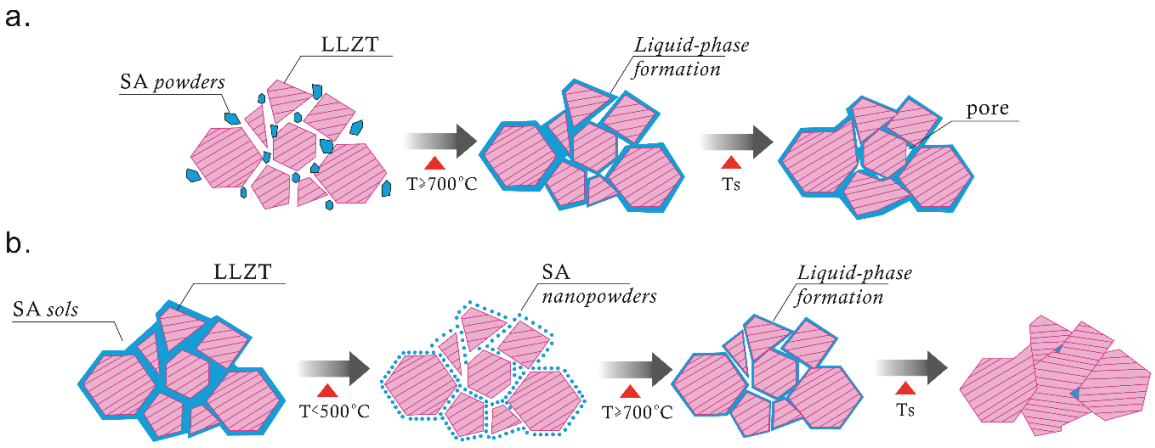

Figure 1. Illustration of the liquid-phase sintering assisted by the (a) powder and (b) solution-process-derived sintering additives. T and T_s are the temperature (during heating) and sintering temperature, respectively.

Figure 1 illustrates the liquid-phase sintering assisted by the powder and solution-process-derived sintering additives. The major difference between the two procedures is that the use of a solution-process-derived sintering additive could provide a more uniform mixing between solid electrolyte particles and sintering additive because of its fluidity compared to those added in the powder-state. The smaller particles of the sintering additive forming a coating on the solid electrolyte particles, after solvent removal, are expected to enhance the liquid-phase sintering even at a small addition amount. Subsequently, liquid-phase sintering occurs, as described above.

Figure S1 shows scanning electron microscopy (SEM) images and X-ray diffraction (XRD) patterns of the LLZT powder used to evaluate the effect of the sintering additives. The morphology of the LLZT powder shows agglomerated particles with sizes between 5 and 20 μm and secondary particle sizes of approximately 1 μm. The XRD pattern matches well with a low-temperature garnet-type cubic phase with the $Ia\bar{3}d$ space group (ICSD #183607) and lattice parameter of a =12.887(4) Å. La_2O_3 was the major secondary phase. The intermediate $La_2Zr_2O_7$ pyrochlore phase could also be present in a lower amount [4, 16], following the general reaction for LLZ usually obtained by the sol–gel process,

$$7Li_2CO_3 + La_2O_3 + 2La_2Zr_2O_7 \rightarrow 2Li_7La_3Zr_2O_{12} + 7CO_2. \quad (1)$$

The precursors of $75Li_2O{\cdot}25B_2O_3$ and Al_2O_3 sintering additive were obtained by a sol–gel process (referred to as LBO and Al_2O_3 sols, respectively) because nanoscale sintering additive precursors in a solution system can be easily obtained by mixing the metal alkoxide or salts and uniformly distributed on the LLZT particles. The following cases were evaluated: (i) LBO and Al_2O_3 in the powder states, (ii) LBO in the sol state and Al_2O_3 in the powder state, and (iii) LBO and Al_2O_3 in the sol states (LLZT-PP, LLZT-SP, and LLZT-SS, denoting the state of each additive (powder or sol), respectively). Figures 2a and 2b show SEM images of the LBO and Al_2O_3 powders, respectively. Agglomerates (approximately 50 μm) with secondary particle sizes below 5–10 μm were observed for the LBO powder, while the Al_2O_3 powder exhibited an average particle size of approximately 1 μm. The in-situ precipitation of LBO and Al_2O_3 from sols is expected in glassy phases with a smaller particle size (nanoscale) (Figure 1b).

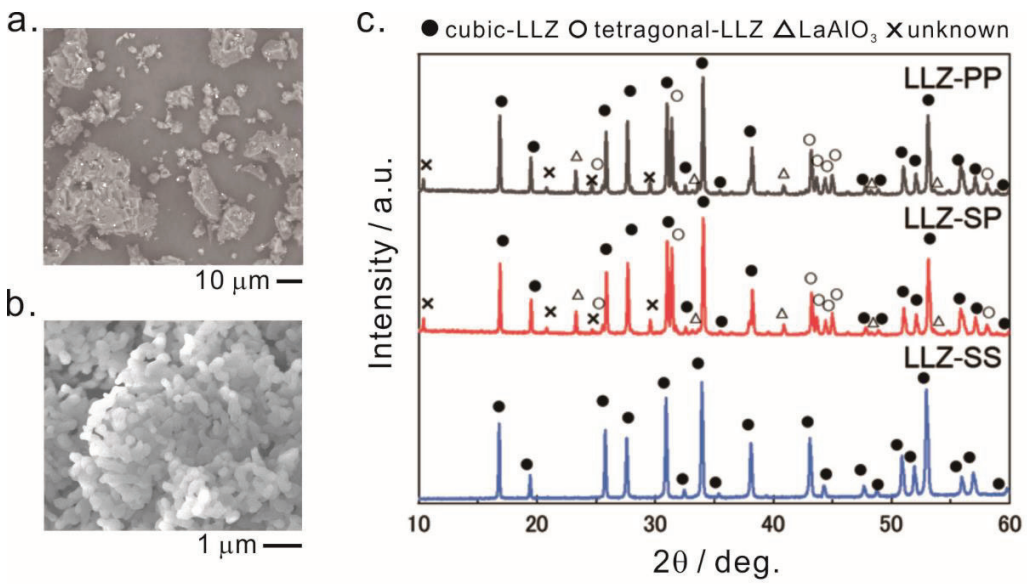

Figure 2. a,b) SEM images of the LBO and Al_2O_3 powders, respectively. c) XRD patterns of LLZT-PP, LLZT-SP, and LLZT-SS sintered at 1000 °C.

Figure 2 shows the XRD patterns of LLZT-PP, LLZT-SP, and LLZT-SS sintered at 1000 °C. The cubic phases with the $Ia\bar{3}d$ space group (ICSD #183607) were the main phases with lattice parameters of 12.898(5), 12.905(4), and 12.930(2) Å for LLZT-PP, LLZT-SP, and LLZT-SS, respectively. LLZT-PP and LLZT-SP exhibited other peaks attributed to the tetragonal phase with the $I4_1/acd$ space group (ICSD #238686), $LaAlO_3$, and unidentified phases. The transition to the tetragonal phase is associated with the insufficient stabilization of the cubic phase, which suggests a nonuniform distribution of the sintering additives or insufficient amount of them, which could be the main reason for the promotion of secondary reactions during sintering. Nonetheless, the addition of solution-derived sintering additives leads to a single-phase cubic garnet structure with a lattice parameter in good agreement with

that of LLZT (12.94 Å) [1, 2]. This confirms that the liquid phase of sintering additives formed during the sintering remains almost unreactive with LLZT grains and is present in the sintered ceramic body as an amorphous phase.

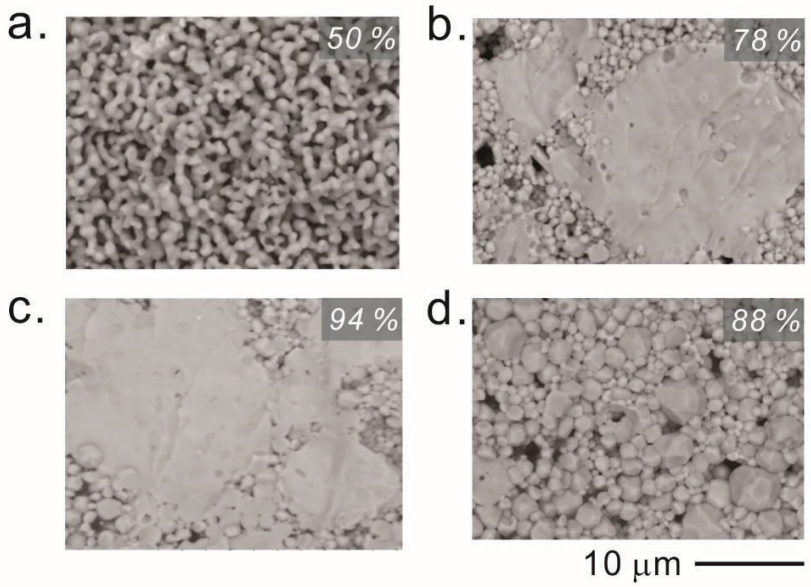

Figure 3. Cross-section SEM images of a) LLZT, b) LLZT-PP, c) LLZT-SP, and d) LLZT-SS sintered at 1000 °C.

Figure 3 shows cross-sectional SEM images of the LLZT pellets without and with sintering additives, including the relative densities. The relative densities of LLZT, LLZT-PP, LLZT-SP, and LLZT-SS were 50%, 78%, 94%, and 88%, respectively. LLZT sintered in the absence of sintering additives exhibited a porous microstructure with single particles with a

size of approximately 1 μm, indicating an insufficient densification. In contrast, the sintering additives positively contributed to the LLZT densification, where larger grains (above 20 μm) were observed as a clear signal of the grain growth and enhanced sintering. Notably, the relative densities of LLZT-PP and LLZT-SP were over- and under-estimated because these samples contained secondary phases (Figure 2b).

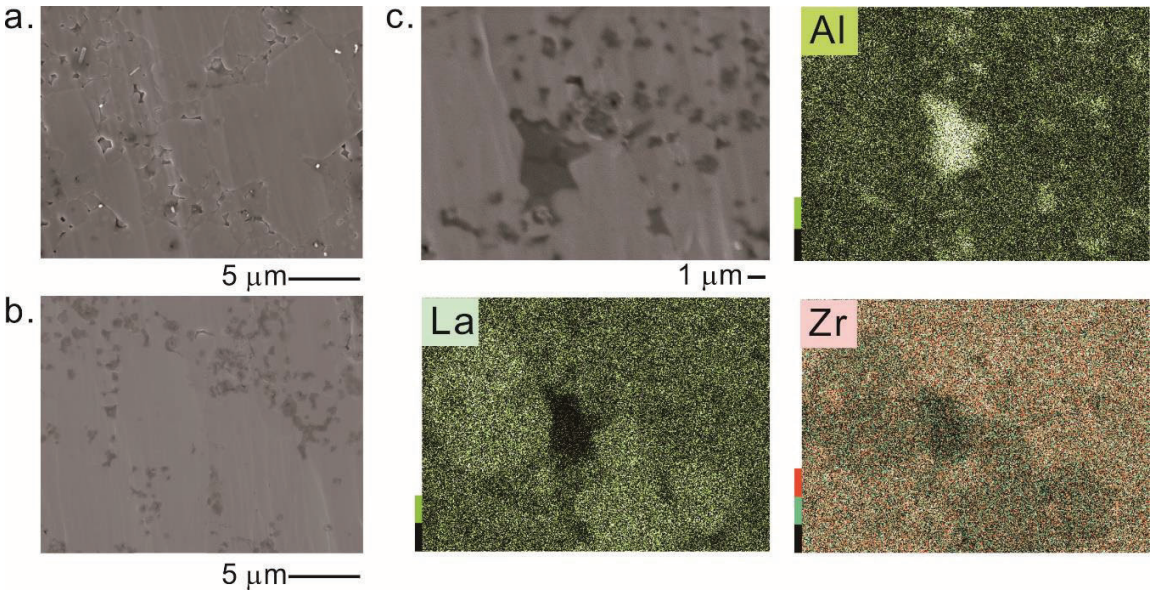

Figure 4. a,b) Cross-section SEM images of LLZT-SS (polished surface). c) Energy-dispersive spectroscopy (EDS) analysis, including composition mapping of aluminum, lanthanum, and zirconium.

The detailed microstructure of LLZT-SS was investigated by SEM–EDS on the cross-section polished surface, as shown in Figure 4. Particles larger than 20 μm in intimate contact with

smaller grains (approximately 1 μm) were observed. In some regions of the surface, dark regions were observed between the grains (Figure 4b). The EDS analysis (Figure 4c) shows that these areas correspond mostly to aluminum-derived compounds, which suggests that they are located at the triple point grain boundaries, as expected. Lithium-borate-derived compositions are also expected to be a part of these dark regions. Similar observations have been reported for LLZ composite electrolytes containing LBO [4]. Notably, the use of LLZT (commercialized powder) with almost negligible secondary phases and sintering with LBO and Al_2O_3 sols under the same conditions did not achieve a sufficient densification (63%, Figure S2), which suggests that the liquid-phase formation during sintering is more complex than expected. Intermediate liquid phases are formed between LBO and La_2O_3 at temperatures around 700 °C [18], which results in a considerable enhancement in the ceramic densification and facilitates the excess consumption of lanthanum oxide in the calcined LLZT powder (Figure S1).

Figures 5a and b show Nyquist plots of the electrochemical impedance of the LLZT pellets with sintering additives measured at 25 °C. The semicircles at high frequencies (>10 kHz) are associated to the resistance of the LLZT composite electrolyte involving grains and grain boundaries. The tail at low frequencies is attributed the stainless-steel blocking electrodes. The wide semicircle of LLZT-PP suggests that most of the contribution of the impedance corresponds to the high resistance of the grain boundaries [4] because of the poor densification or series of highly resistive components generated by the secondary phases through the pellet. The depletion of the semicircle of LLZT-SP at high frequencies (1 MHz) is associated with the better densification allowing the separation between grain and grain

boundary resistances in good agreement with LLZ garnet electrolytes sintered with and without sintering additives in which grain resistance contribution is observed between ca. 1 MHz–1 GHz [8, 19]. The same separation can be observed in the impedance profile (Figure 5b) of LLZT-SS with a major contribution at higher frequencies (1–3 MHz) and almost negligible contribution at intermediate frequencies (1–0.1 MHz), which suggests that most of the impedance corresponds to the lithium-ion transport through the LLZT grains with a negligible contribution of grain boundaries.

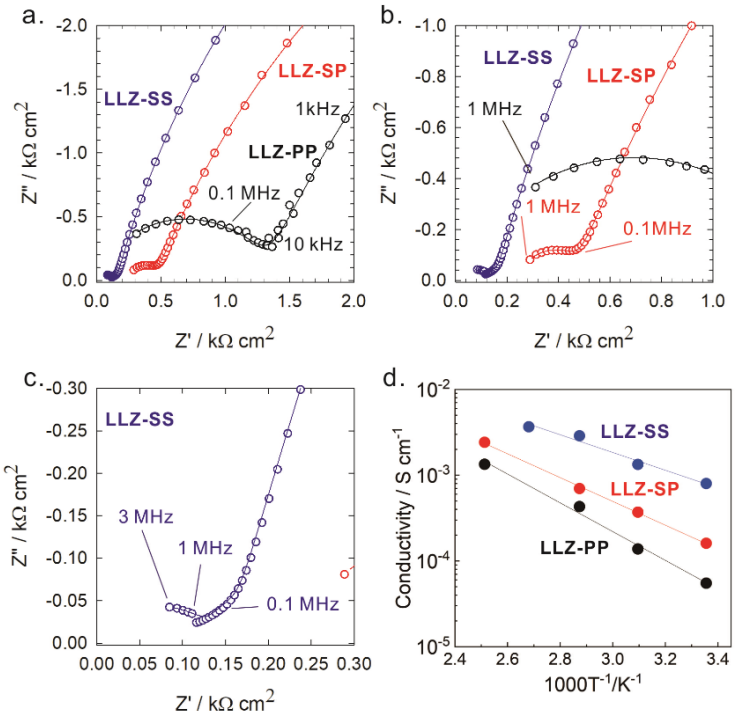

Figure 5. a-c) Nyquist plots of LLZT pellets with sintering additives at room temperature. Open circles represent the measured data, and solid lines indicated the fit of the data. Information of fitting to the equivalent circuit is provided in Figure S3. d) Arrhenius plot of LLZT pellets obtained by the total ionic conductivity.

The total ionic conductivity (grain + grain boundary) calculated by the fitting of impedance profiles to the equivalent circuits (Figure S3, Table SI) was 0.063, 0.16, and 0.8 mS cm^{-1} for LLZT-PP, LLZT-SP, and LLZT-SS, respectively. The grain and grain boundary resistances of LLZT-SS was 136.3 and 17.5 Ω.cm (Figure S3c, Table SI), respectively. Thus, the grain conductivity in LLZT-SS was estimated to be approximately 90% of the total conductivity, higher than that in LLZT-SP (46%).

Figure 5b shows an Arrhenius plot of the LLZT pellets obtained by the total ionic conductivity in the temperature range of 25–125 °C. The activation energy was 14, 12, and 9 kJ mol^{-1} for LLZT-PP, LLZT-SP, and LLZT-SS, respectively. The lowest activation energy obtained when LLZT is sintered with LBO and Al_2O_3 sols is attributed to the low resistance of the grain boundaries. In other words, the ion mobility through the grain boundaries, formed by a more uniform distribution of sintering additives presumably located at the grain boundaries, is facilitated by the good contact between the LLZT grains and sintering additives. Moreover, the activation energies of all LLZT pellets sintered with sols or powders are lower than the reported activation energies for Al, Ta-doped LLZ (~30 kJ mol^{-1}) [1] which suggests the formation of almost Al-undoped LLZT grains. ~~attributed to~~ The intragranular ionic conductivity of the Al-free LLZT solid electrolytes~~, which~~ can exhibit activation energies as low as 10 kJ mol^{-1} [20]. This is in good agreement with the EDS analysis (Figure 4c), which suggest that the Al_2O_3 sol is located mainly at the triple points grain boundaries and presumably along the grain boundaries between LLZT particles.

Table I compares reported LLZ composite electrolytes prepared by the addition of LBO with/without Al_2O_3 sintering additives and that prepared in this study. The liquid-phase formation during the sintering was promoted by reducing the particle size of LBO using several grindings and multi-step heating. However, the required amount of LBO cannot be lower than ~4.5 - 10 wt% to achieve a sufficient densification. The considerable reduction of LBO (2 wt%) reported by Jonson and McGinn [12] has been achieved by sintering a Nb-doped LLZ under an argon atmosphere, where LBO is effective in forming the liquid phase during sintering without compensating the liquid loss from the LLZ composition, which usually occurs under oxygen or atmospheric conditions. Nevertheless, the ionic conductivity of LLZ solid electrolytes containing LBO phases seems to be not higher than 0.1–0.5 mS cm^{-1} with a significant contribution of the grain boundaries (up to 50%) and high activation energies of approximately 28–40 kJ mol^{-1} [4, 8, 15, 21].

Table I. LLZ composite electrolytes prepared by addition of LBO and Al_2O_3.

Garnet-type solid electrolyte	LBO (wt%)	Al_2O_3 (mol%)	ST (ºC)	Conductivity (mS cm^{-1})	Reference / year
Ca/Nb-doped LLZ	10 vol.%	0.2	800	0.36 (25 ºC)	[8] / 2014
Nb-doped LLZ	2*	0.1	1000	0.25 (NS)	[12] / 2018
Ta-doped LLZ	6.3	NS	1000	0.55 (30 ºC)	[13] / 2019
Ta-doped LLZ	20 vol.% **	NS	1000	0.23 (27 ºC)	[14] / 2020
LLZ	10	2.4 at%	850	0.14 (NS)	[15]/ 2020
Ta-doped LLZ	0.5 (1.2 vol.%)	0.2	1000	0.80 (25 ºC)	This study

The presented LLZ pellets are comparable in terms of relative density (approximately 90%). ST: sintering temperature; NS: non specified; *Argon atmosphere; **Li_3BO_3–Li_2CO_3 composite.

We utilized LBO and Al_2O_3 as well-known sintering additives for the LLZT solid electrolytes by varying the processing using the solution-derived sintering additives. The solution-derived sintering additives were highly effective in densifying LLZT and enhancing the lithium-ion transport properties. They provided a high conductivity of 0.8 mS cm^{-1} with a low activation energy (9 kJ mol^{-1}) and almost negligible contribution of grain boundary resistance. The initial composition of the garnet solid electrolyte is crucial to achieve the enhanced properties. The lanthanum oxide was beneficial because it could form liquid phases in the presence of lithium borate during the sintering. Therefore, further modification of the composition of both solid electrolyte and solution-derived sintering additives could provide

materials with even higher conductivities or processing at lower temperatures. Moreover, the proposed approach could significantly reduce the energy consumption of the sintering process and simplify the grinding and heating stages. This process could be also valuable for processing of other ceramic materials.

Conclusions

The effects of $Li_2O–B_2O_3$ and Al_2O_3 solution-derived sintering additives on the sinterability of LLZT solid electrolyte were studied and compared to their powder-state counterparts. The use of solution-derived sintering additives leads to a single-phase cubic garnet structure and enhanced densification. In contrast, the transition to the tetragonal phase garnet structure accompanied with other secondary phases was obtained when powder-state sintering additives were used. The use of 1.2-vol% (0.5 wt%) $75Li_2O{\cdot}25B_2O_3$ and 1.5-vol% Al_2O_3 sintering additives in sintering of LLZT ceramic solid electrolyte achieves a high ionic conductivity of 0.8 mS cm^{-1} at 25 ° with low activation energy (9 kJ mol^{-1}) and almost negligible contribution of the grain boundary resistance (10%).

Acknowledgements

N.C.R.-N. acknowledges financial support by SOUSEI Support Program for Young Researchers in FY2020 of Hokkaido University and partial support from Nippon Sheet Glass Foundation in FY2021. The SEM analysis was carried out with JIB4600F at the “Joint-use

Facilities: Laboratory of Nano-Micro Material Analysis", Hokkaido University, supported by "Material Analysis and Structure Analysis Open Unit (MASAOU)". The authors thank Mr. Keita Suzuki for his assistance with cross-section preparation of ceramic electrolytes for SEM analysis.

References

[1] V. Thangadurai, S. Narayanan, D. Pinzaru, Garnet-type solid-state fast Li ion conductors for Li batteries: critical review, Chem. Soc. Rev. 43 (2014) 4714–4727. DOI: 10.1039/c4cs00020j.

[2] S. Ramakumar, C. Deviannapoorani, L. Dhivya, L.S. Shankar, R. Murugan, Lithium garnets: Synthesis, structure, Li + conductivity, Li + dynamics and applications, Prog. Mater. Sci. 88 (2017) 325–411. DOI: 10.1016/j.pmatsci.2017.04.007.

[3] N.S. Kulkarni, T.M. Besmann, K.E. Spear, Thermodynamic Optimization of Lithia-Alumina, J. Am. Ceram. Soc. 91 (2008) 4074–4083. DOI: 10.1111/j.1551-2916.2008.02753.x.

[4] N.C. Rosero-Navarro, K. Tadanaga, Solid electrolytes for advanced applications, eds. in: M.R. and W.W. Springer International Publishing, Cham, 2019, pp. 111–128. DOI: 10.1007/978-3-030-31581-8_5.

[5] S. Kumazaki, Y. Iriyama, K.H. Kim, R. Murugan, K. Tanabe, K. Yamamoto, T. Hirayama, Z. Ogumi, High lithium ion conductive $Li_7La_3Zr_2O_{12}$ by inclusion of both Al and Si, Electrochem. Commun. 13 (2011) 509–512. DOI: 10.1016/j.elecom.2011.02.035.

[6] K. Tadanaga, R. Takano, T. Ichinose, S. Mori, A. Hayashi, M. Tatsumisago, Low temperature synthesis of highly ion conductive $Li_7La_3Zr_2O_{12}$–Li_3BO_3 composites, Electrochem. Commun. 33 (2013) 51–54. DOI: 10.1016/j.elecom.2013.04.004.

[7] S. Ohta, S. Komagata, J. Seki, T. Saeki, S. Morishita, T. Asaoka, All-solid-state lithium ion battery using garnet-type oxide and Li_3BO_3 solid electrolytes fabricated by screen-printing, J. Power Sources 238 (2013) 53–56. DOI: 10.1016/j.jpowsour.2013.02.073.

[8] S. Ohta, J. Seki, Y. Yagi, Y. Kihira, T. Tani, T. Asaoka, Co-sinterable lithium garnet-type oxide electrolyte with cathode for all-solid-state lithium ion battery, J. Power Sources 265 (2014) 40–44. DOI: 10.1016/j.jpowsour.2014.04.065.

[9] N. Janani, S. Ramakumar, S. Kannan, R. Murugan, Optimization of Lithium Content and Sintering Aid for Maximized Li + Conductivity and Density in Ta-Doped $Li_7La_3Zr_2O_{12}$, J. Am. Ceram. Soc. 98 (2015) 2039–2046. DOI: 10.1111/jace.13578.

[10] N.C. Rosero-Navarro, A. Miura, M. Higuchi, K. Tadanaga, Optimization of Al2O3 and Li_3BO_3 Content as Sintering Additives of Li_{7-x} $La_{2.95}Ca_{0.05}ZrTaO_{12}$ at Low Temperature, J. Electron. Mater. 46 (2017) 497–501. DOI: 10.1007/s11664-016-4924-4.

[11] N.C. Rosero-Navarro, T. Yamashita, A. Miura, M. Higuchi, K. Tadanaga, Effect of Sintering Additives on Relative Density and Li-ion Conductivity of Nb-Doped $Li_7La_3Zr_2O_{12}$ Solid Electrolyte, J. Am. Ceram. Soc. 100 (2017) 276–285. DOI: 10.1111/jace.14572.

[12] R.A. Jonson, P.J. McGinn, Tape casting and sintering of $Li_7La_3Zr_{1.75}Nb_{0.25}Al_{0.1}O_{12}$ with Li_3BO_3 additions, Solid State Ionics 323 (2018) 49–55. DOI: 10.1016/j.ssi.2018.05.015.

[13] H. Xie, C. Li, W.H. Kan, M. Avdeev, C. Zhu, Z. Zhao, X. Chu, D. Mu, F. Wu, Consolidating the grain boundary of the garnet electrolyte LLZTO with Li_3BO_3 for high-performance $LiNi_{0.8}Co_{0.1}Mn_{0.1}O_2$ /$LiFePO_4$ hybrid solid batteries, J. Mater. Chem. A 7 (2019) 20633–20639. DOI: 10.1039/C9TA03263K.

[14] H. Hosokawa, A. Takeda, R. Inada, Y. Sakurai, Tolerance for Li dendrite penetration in Ta-doped $Li_7La_3Zr_2O_{12}$ solid electrolytes sintered with $Li_{2.3}C_{0.7}B_{0.3}O_3$ additive, Mater. Lett. 279 (2020). DOI: 10.1016/j.matlet.2020.128481, 128481.

[15] J. Han, J.C. Kim, A solid-state route to stabilize cubic $Li_7La_3Zr_2O_{12}$ at low temperature for all-solid-state-battery applications, Chem. Commun. (Camb. U.K.) 56 (2020) 15197–15200.

[16] N.C. Rosero-Navarro, T. Yamashita, A. Miura, M. Higuchi, K. Tadanaga, Preparation of $Li_7La_3(Zr_{2-x},Nb_x)O_{12}$ (x= 0–1.5) and Li_3BO_3/$LiBO_2$ composites at low temperatures using a sol–gel process, Solid State Ionics 285 (2016) 6–12. DOI: 10.1016/j.ssi.2015.06.015.

[17] L.F. Maia, A.C.M. Rodrigues, Electrical conductivity and relaxation frequency of lithium borosilicate glasses, Solid State Ionics 168 (2004) 87–92. DOI: 10.1016/j.ssi.2004.02.016.

[18] A. Bohac, A. Gauman, NIST Phase Equilibria Diagrams, 1980.

[19] W. E. Tenhaeff, E. Rangasamy, Y. Wang, A. P. Sokolov, J. Wolfenstine, J. Sakamoto and N. J. Dudney, Resolving the Grain Boundary and Lattice Impedance of Hot-Pressed $Li_7La_3Zr_2O_{12}$ Garnet Electrolytes, ChemElectroChem, 1 (2014), 375-378. DOI: https://doi.org/10.1002/celc.201300022

[20] M. Matsui, K. Takahashi, K. Sakamoto, A. Hirano, Y. Takeda, O. Yamamoto, N. Imanishi, Phase stability of a garnet-type lithium ion conductor $Li_7La_3Zr_2O_{12}$, Dalton Trans. 43 (2014) 1019–1024. DOI: 10.1039/c3dt52024b.

[21] L.C. Zhang, J.F. Yang, Y.X. Gao, X.P. Wang, Q.F. Fang, C.H. Chen, Influence of Li_3BO_3 additives on the Li+ conductivity and stability of Ca/Ta-substituted $Li_{6.55}(La_{2.95}Ca_{0.05})(Zr_{1.5}Ta_{0.5})O_{12}$ electrolytes, J. Power Sources 355 (2017) 69–73. DOI: https://doi.org/10.1016/j.jpowsour.2017.04.044

Supporting Information

Synthesis of highly Li-ion conductive garnet-type solid ceramic electrolytes by solution-process-derived sintering additives

Nataly Carolina Rosero-Navarro[a*], Haruna Watanabe[b], Akira Miura[a] and Kiyoharu Tadanaga[a]

[a]Division of Applied Chemistry, Faculty of Engineering, Hokkaido University, Sapporo 060–8628, Japan

[b]Graduate School of Chemical Sciences and Engineering, Hokkaido University, Sapporo 060–8628, Japan

*E-mail address: rosero@eng.hokudai.ac.jp

Experimental Section.

1.1 Synthesis

Ta-doped LLZ solid electrolyte

The synthesis of Ta-doped LLZ by the sol-gel process was carried out following a reported procedure[1]. First, $LiNO_3$ (99%, Kanto chemicals) and $La(NO_3)_3 \cdot 6H_2O$ (99.9%, Kanto chemicals) were dissolved in ethanol. Second, $Ta(OC_2H_5)_5$ (99.9%, High-purity chemicals), $Zr(OC_4H_9)_4$ (85% in butanol, Wako pure chemicals) and ethyl acetoacetate (EAcAc, 99%, Kanto chemicals) were dissolved in ethanol under argon atmosphere and stirred for 1 hour. Then, both solutions were mixed, and the resulted transparent solution was stirred at room temperature for 1 to 2 hours to obtain a sol. The obtained sol was dried under vacuum between 80 and 130 °C to obtain a dried gel that was later pulverized and heat-treated at 700 °C in an alumina crucible for 5 hours (1 °C min^{-1}). Finally, 2 g of this powder and 4 mL of toluene were placed in a ZrO_2 pot and grounded at 300 RPM for 6 hours. Then, toluene was evaporated under vacuum at 100 °C to obtain final LLZT calcined powder. The molar ratio of Li:La:Zr:Ta:EAcAc was 7.15:3:1.3:0.5:1.5 and lithium was added in 10% excess to compensate for the loss of Li during sintering.

Sintering additives

The Al_2O_3 sol and powder were obtained by commercial source with particle size ~ 50 nm and ~ 1 μm, respectively. Both materials were used without any further purification or pretreatment.

The Li_2O-B_2O_3 sol was synthesized by the sol-gel process using trimethoxyborane (TMB, Shin-Etsu Chemicals) and lithium ethoxide (High-purity chemicals) in a molar ratio 3:1 and total concentration of 40 gL^{-1}. TMB was dissolved in ethanol and stabilized by addition of EAcAc under argon atmosphere. Then, 0.1 M HNO_3 was added dropwise (molar ratio TMB:HNO_3 of 1:0.5), and the mixture was stirred for 1 hour. In parallel, lithium ethoxide was dissolved in ethanol. Then, both solutions, TMB and lithium ethoxide, were mixed and stirred for 1 hour to obtain a precursor LBO solution.

The LBO powder was synthesized by the solid-state process following a reported procedure[1, 2]. Briefly, the Li_2O (Wako pure chemicals) and B_2O_3 (Wako pure chemicals) in a molar ratio 3:1 were ball milled under an argon atmosphere for 40 hours under 370 RPM. Then, the milled powder was heat-treated at 210 ° C for 10 hours and finally to 600 ° C for 5 hours to obtain Li_3BO_3 powder.

Sintering of LLZT pellets

The sintering additives, sols and/or powders, were added to the LLZT calcined powder and mixed in a mortar using toluene. Toluene was completely removed at 80 °C for approximately 2 hours. The calcinated LLZT powder containing sintering additives were formed into pellets (Ø = 10 mm) at 100 MPa (5 min) using a uniaxial press and then, were sintered at 1000 ºC (10 h) using a heating rate of 1 ºC/min and intermedium step at 700 ºC (5 h). The pellets were sintered under ambient atmosphere using alumina crucibles. The pellets were thoroughly buried in identical powder to mitigate losses of lithium and prevent any contamination with crucibles.

1.2 Characterization

Crystal phase was determined by X-ray diffraction (XRD) using a RINT 2000 Ultima RIGAKU diffractometer. Powder samples were scanned between 10º and 60º at a rate of 2°/min using Cu-Kα radiation. Morphology of the cross-section pellets were observed by scanning electron microscopy (SEM), performed on a MultiFlex600 and JIB-4600F Multibeam SEM-FIB Scanning Electron Microscopes.

The relative density was calculated with a geometrical dimension of the pellets and theoretical density of LLZT (5.11 g cm^{-3}). HS Flat Cell HS-3ETK (Hohsen Corporation) was used to perform the electrochemical measurements. The conductivity of the composite solid electrolyte pellets was evaluated by the electrochemical impedance spectroscopy (EIS), under Ar atmosphere. The samples were Au-coated and sandwiched between two stainless-steel (SS, blocking electrodes) disks used as current collectors. EIS measurements were conducted using an impedance analyzer (SI 1260, Solartron) in the frequency range of 1-3 MHz to 100 Hz at the amplitude of 80-100 mV. The impedance spectra were analyzed with ZView (Scribner Associates) to assess the ohmic total resistance (Rt), which was normalized to the pellet geometry (t: thickness and A: golden surface area) to calculate the conductivity through the usual formula $\sigma = t / R_t.A$.

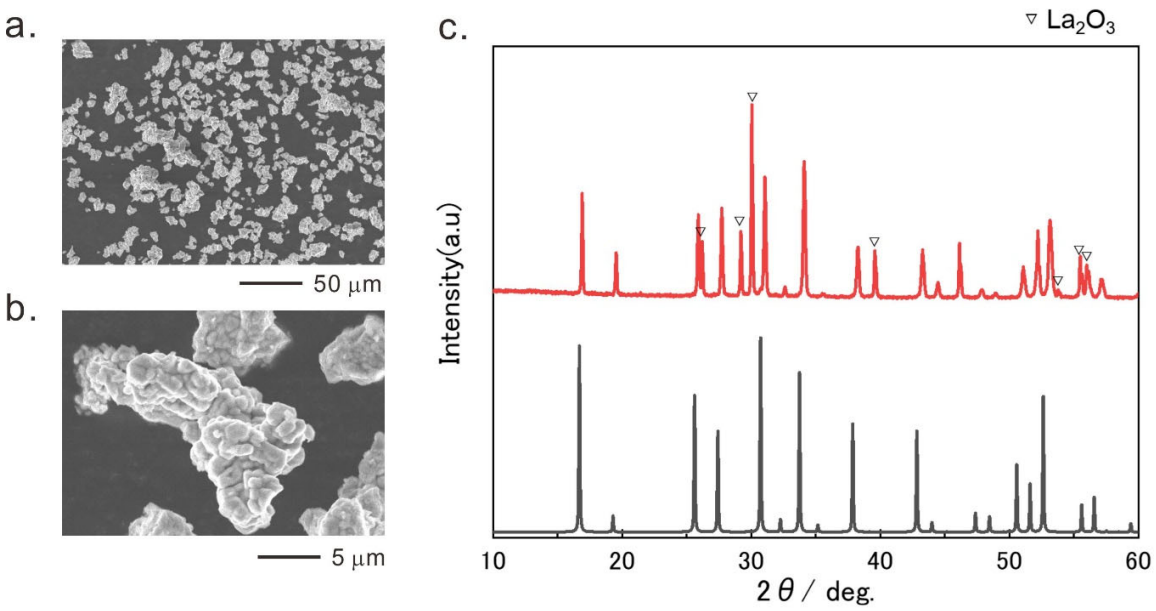

Figure S1. a-b) SEM of LLZT calcinated powder. c) XRD pattern of LLZT calcinated powder compared (Top) with LLZ cubic phase (Bottom) with the $Ia\bar{3}d$ space group (ICSD #183607).

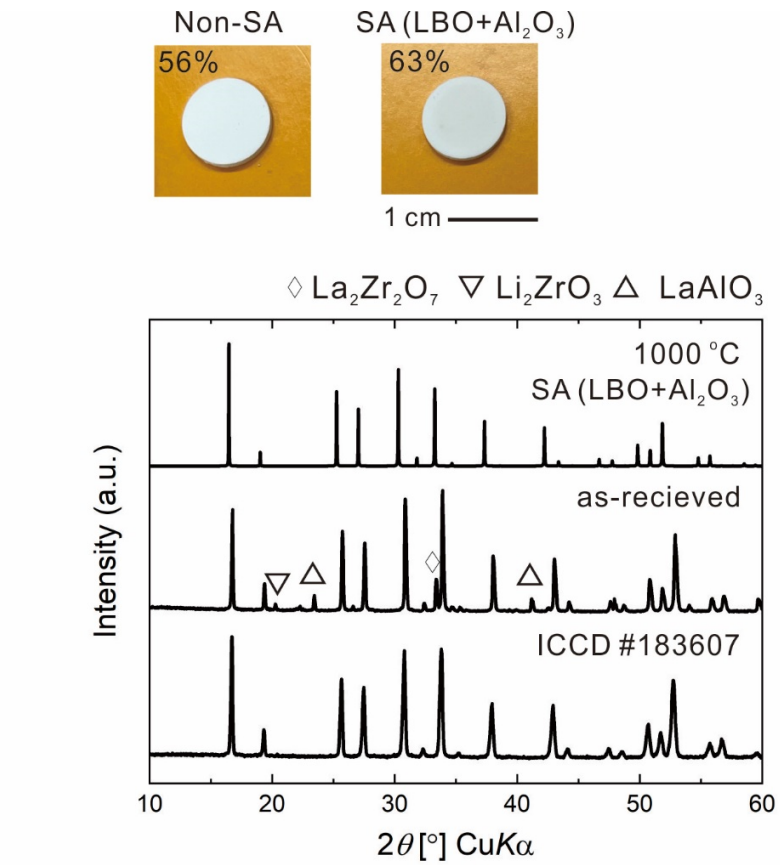

Figure S2. XRD pattern of a) $Li_{6.6}La_3Zr_{1.6}Ta_{0.4}O_{12}$ powder (commercialized by Toshima, average particle size: 5 μm) and after sintering using LBO and Al_2O_3 sols as sintering additives. LLZ cubic phase was also included as reference (ICSD #183607).

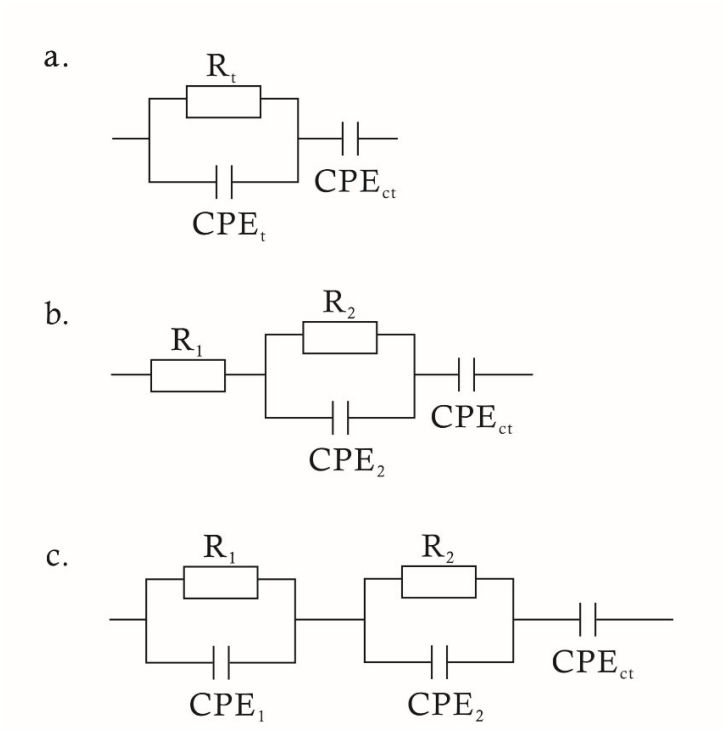

Figure S3. Equivalent Circuits used to fit the impedance profile of a) LLZT-PP, b) LLZT-SP, and c) LLZT-SS. This should be noted that limited information at high frequencies can induce uncertainty in the assigned values for the contributions of grain and grain boundary resistances. To reduce the error, the equivalent circuits used to fit the impedance profiles are the simplest solution possible. The goodness of fit remains in the order of 10^{-5}. R represents the resistance and CPE the constant phase element, which is characterized by two parameters C and n. The capacitance can be calculated from $CPE = (R^{1-n}C)^{1/n}$. Rt (CPEt) is used to simulate the total resistance containing grain and grain boundary resistances in equivalent circuit a. R_1 (CPE1) and R_2 (CPE2) are assigned to grain and grain boundary resistances, respectively in equivalent circuits b and c. CPEct is used to simulate the charge transference due to stainless steel electrodes.

Table SI. Fitting results of impedance profiles (Figure 5) of LLZT-PP, LLZT-SP, and LLZT-SS using equivalent circuits in Figure S2.

Sample	R1 (Ω.cm)	R2 (Ω.cm)	RTotal (Ω.cm)	CPE1 (F)	CPE2 (F)	CPEt (F)	CPEct (F)	*n*
LLZT-PP	-	-	1319	-	-	2×10^{-9}	2×10^{-7}	0.76
LLZT-SP	246.1	210.3	456.4	-	1×10^{-9}	-	1×10^{-7}	0.78
LLZT-SS	136.3	17.5	153.8	1×10^{-10}	4×10^{-9}	-	1×10^{-7}	0.83

References

1. N. C. Rosero-Navarro, A. Miura, M. Higuchi and K. Tadanaga, *Journal of Electronic Materials*, 2017, **46**, 497-501.
2. N. C. Rosero-Navarro, T. Yamashita, A. Miura, M. Higuchi and K. Tadanaga, *Solid State Ionics*, 2016, **285**, 6-12.